On the Irreducible Brillouin Zones of 1D Glide-Symmetric Structures

On the Irreducible Brillouin Zones of 1D Glide-Symmetric Structures

M. Petek[(1)], J. A. Tobon Vasquez[(1)], G. Valerio[(2)], F. Mesa[(3)], O. Quevedo-Teruel[(4)], and F. Vipiana[(1)]

[(1)] Dept. of Electronics and Telecommunications, Politecnico di Torino, 10129, Torino, Italy
{martin.petek, jorge.tobon, francesca.vipiana}@polito.it
[(2)] Sorbonne Université, CNRS, Laboratoire de Génie Électrique et Électronique de Paris (GeePs), 75252, Paris, France
Université Paris-Saclay, CentraleSupélec, CNRS, GeePs, 91192, Gif-sur-Yvette, France
[(3)] Dept. Física Aplicada 1, Universidad de Sevilla, Seville, Spain
[(4)] KTH, Division of Electromagnetic Engineering and Fusion Science, 11428, Stockholm, Sweden

***Abstract*—This paper discusses the appropriate choice of the irreducible Brillouin zone for one-dimensional (1D) glide-symmetric structures in a 2D square lattice. In analyzing the dispersion diagrams, we analytically show that the positive and negative branches of the solutions are identical, representing the same solution derived from different parts of the Brillouin zone. We then propose an alternative path accounting for the glide periodicity, which is easier to understand and helps to better interpret dispersion diagrams. Our proposal is validated with the help of a linearized half-cell multimodal transfer matrix method, which allows us to obtain solutions more efficiently as the computational domain is reduced by half.**

I. Introduction

Periodic structures are used in electromagnetics for numerous applications, so they have been the focus of extensive investigations [1]–[3]. Recently, it has been rediscovered that glide symmetry can introduce some advantages with respect to conventional periodic structures [4]. Given their practical interest, several specialized numerical methods have been proposed for the analysis of glide-symmetric structures [5], [6], including some works by the authors of this paper [7]–[9]. These structures are characterized by the glide periodicity, that is, the structure is periodic with respect to a translation by half a period and a mirroring [10], [11].

In this work, we discuss the appropriate irreducible Brillouin zone (IBZ) for 2D-periodic structures which possess glide periodicity in only one of the directions, as in the cases studied in [12], [13]. We argue that a more advantageous path through the Brillouin zone can be identified to understand the structure's properties more effectively than that shown in earlier studies. To demonstrate this concept, we also present a linearized formulation of the multi-modal transfer matrix method (MMTMM) [14], which allows reducing the size of the unit cell based on glide periodicity [8] and, in addition to being more computationally efficient, helps understand the physical properties of the structure.

II. Theoretical consideration

For any given 2D-periodic structure with a periodicity p in x and y, Floquet's theorem states that the electric field $\mathbf{E}$ after a translation can be obtained by [8], [15]:

$$\mathbf{E}(x+p, y+p, z) = \mathrm{e}^{-\mathrm{j}k_x p}\mathrm{e}^{-\mathrm{j}k_y p}\mathbf{E}(x,y,z)\ . \tag{1}$$

As a consequence, when we search for modal solutions, it is sufficient to only obtain the solutions with wavevector components within the region values of $k_x, k_y \in [-\pi/p, \pi/p]$ which are unique, since

$$\mathrm{e}^{-\mathrm{j}p(k_x + 2n\pi/p)} = \mathrm{e}^{-\mathrm{j}pk_x}, \qquad n = \pm 1, \pm 2, \ldots \tag{2}$$

This region is referred to as the first Brillouin zone [15]. If the periodic structure has symmetries, the first Brillouin zone can be reduced further. The smallest region of unique solutions is named the IBZ [15]. Typically, solutions are presented only at the boundary of the IBZ, as in many cases they provide a sufficient understanding of the structure [8], [15], [16].

For glide-symmetric structures, the Floquet theorem can be generalized to account also for glide symmetry [7], [11]. For a structure with glide symmetry only along the axis x, it can be written as

$$\mathbf{E}\big(x+\hat{p}, y, -z\big) = \pm\mathrm{e}^{-\mathrm{j}k_x\hat{p}}\mathbf{E}(x,y,z) \tag{3}$$

$$\mathbf{E}\big(x, y+p, z\big) = \mathrm{e}^{-\mathrm{j}k_y p}\mathbf{E}(x,y,z) \tag{4}$$

where $\hat{p} = p/2$ is the glide periodicity and the $\pm$ arises when a square root is taken in the derivation [8], [11]. In [8], [9], this fact is used to reduce the unit cell and both $\pm$ branches are explored for solutions. Here, we make the argument that the "$+$" and "$-$" branches are, in fact, the same solution, sampled in different parts of the Brillouin zone. Consider the Euler identity:

$$-1 = \mathrm{e}^{-\mathrm{j}\pi} = \mathrm{e}^{-\mathrm{j}(\pi/\hat{p})\hat{p}} = \mathrm{e}^{-\mathrm{j}k_s\hat{p}}\ . \tag{5}$$

If (5) is inserted into (3)

$$\mathbf{E}\big(x+\hat{p}, y, -z\big) = \begin{cases} \mathrm{e}^{-\mathrm{j}k_x\hat{p}}\mathbf{E}(x,y,z) \\ \mathrm{e}^{-\mathrm{j}(k_x+k_s)\hat{p}}\mathbf{E}(x,y,z) \end{cases} \tag{6}$$

we can observe that taking the "$-$" branch is equivalent to scanning the Brillouin Zone with the value of k_x shifted by $k_s = \pi/\hat{p}$. However, common electromagnetic solvers do not contain a glide-periodic boundary condition. Instead, periodic boundary conditions are used. If we translate twice by $\hat{p}$, we again obtain the Floquet theorem:

$$\mathbf{E}\big(x+p, y, z\big) = \begin{cases} \mathrm{e}^{-\mathrm{j}k_x p}\mathbf{E}(x,y,z) \\ \mathrm{e}^{-\mathrm{j}(k_x+k_s)p}\mathbf{E}(x,y,z) \end{cases}\ . \tag{7}$$

TABLE I
WAVE VECTOR VALUES AT EDGES OF THE IBZ

Commonly scanned path Periodic boundary conditions		
Point	k_x	k_y
Γ	0	0
X	π/p	0
M	π/p	π/p
Y	0	π/p

Proposed path Glide boundary conditions		
Point	k_x	k_y
Γ	0	0
$\mathrm{X_G}$	$2\pi/p = \pi/\hat{p}$	0
$\mathrm{M_G}$	$2\pi/p = \pi/\hat{p}$	π/p
Y	0	π/p

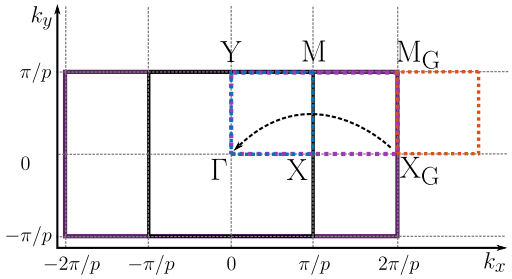

Fig. 1. Paths in the Brillouin zone. The dotted lines represent the scanned paths of the "+" branch (dotted blue), "−" branch (dotted orange) and the proposed path (dotted violet). The dashed arrow represents the mirroring of the apparent position of the " − " path when the structure is analyzed with the periodic boundary conditions.

Therefore, the added phase shift of k_x for the "−" mode turns out to be 2π when the structure is analyzed using periodic boundary conditions ($k_s p = 2\pi$). In this case, when we scan the commonly used path $\overline{\Gamma\mathrm{XMY\Gamma}}$, as defined on the left of Table I and depicted as a blue dotted line in Fig. 1, we additionally obtain the solution of the "−" branch, the orange dashed line. Since the "−" branch of the path does not lie in the first Brillouin zone, it is an extra mode, and applying the simulation setup using (1) is equivalent to the case where a supercell is used in the simulation [17]. Therefore, in the direction of the glide periodicity, we instead propose to consider $\hat{p}$ as the periodicity of the structure and to scan the path $\overline{\Gamma\mathrm{X_G M_G Y\Gamma}}$. This path is defined on the right of Table I and depicted in dotted violet line in Fig. 1. Then, only the "+" mode should be kept, as it contains the complete information on the properties of the structure.

III. MMTMM ANALYSIS

To further demonstrate the theory, we here describe an efficient MMTMM scheme, capable of setting the periodic and glide-periodic boundary condition. The MMTMM analysis is carried out in two steps. First, the coupling matrix of the port modes, defined at the boundary of the unit cell is obtained. Each port contains multiple port modes [16]. The solver used is CST Frequency Domain Solver (CST FDS) with hexahedral meshing, as it allows for placing an open boundary condition on the port boundaries. Then, the eigenvalues are obtained with a postprocessing procedure [16] by solving the following

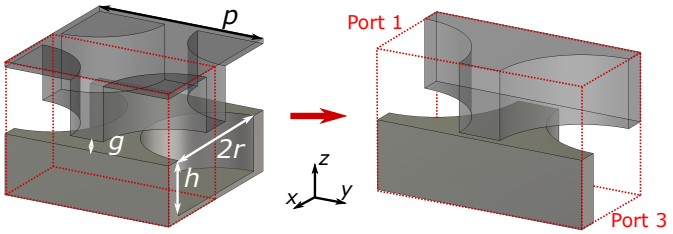

Fig. 2. Studied geometries: the glide-symmetric unit cell (left) and the half-cell (right).

eigenvalue problem:

$$[\widetilde{\mathbf{T}}]\begin{bmatrix}\mathbf{F}_x\\ \mathbf{F}_y\end{bmatrix} = [\mathbf{P}]\begin{bmatrix}\pm\lambda_x\mathbf{F}_x\\ \lambda_y\mathbf{F}_y\end{bmatrix} \tag{8}$$

where $[\widetilde{\mathbf{T}}]$ is the permuted transfer matrix [14], $\mathbf{F}_\nu$ (with ν either x or y) is the vector of equivalent port voltages $\mathbf{V}_\nu$ and currents $\mathbf{I}_\nu$ defined as

$$[\widetilde{\mathbf{T}}] = \begin{bmatrix}[\widetilde{\mathbf{T}}_{xx}] & [\widetilde{\mathbf{T}}_{xy}]\\ [\widetilde{\mathbf{T}}_{yx}] & [\widetilde{\mathbf{T}}_{yy}]\end{bmatrix} \quad , \quad \mathbf{F}_\nu = \begin{bmatrix}\mathbf{V}_\nu\\ \mathbf{I}_\nu\end{bmatrix} . \tag{9}$$

The eigenvalues λ_ν are defined as $\lambda_\nu = \exp(-\mathrm{j}k_\nu p_\nu)$ with k_ν being the wavevector component and p_ν the periodicity of the structure in the ν direction. Since we are using a half-cell in Fig. 2(a), which has half periodicity in x, we additionally introduce a factor of ± 1 at λ_x [8] in (8), which stand for the "+" or "−" branches in (3). The matrix $[\mathbf{P}]$ is a diagonal matrix with elements of $+1$ or -1 that describe the mode z parity of two opposite ports ($\underline{\mathbf{Q}}$ in [8]). This matrix corrects for a possible 180° phase shift after the appropriate geometrical transformation (periodic or glide-periodic) between two opposite ports, which can be identified by checking the z component of the electric field for each port mode [8]. Note that both x- and y- aligned ports must be checked, whether they are at a glide-periodic or a periodic boundary.

To efficiently solve (8), we first left-multiply with $[\mathbf{P}]$, noting $[\mathbf{P}]^{-1} = [\mathbf{P}]$ and define the following half-cell transfer matrix $[\widetilde{\mathbf{T}}_{\frac{1}{2}}]$:

$$[\widetilde{\mathbf{T}}_{\frac{1}{2}}] = [\mathbf{P}][\widetilde{\mathbf{T}}] = \begin{bmatrix}[\widetilde{\mathbf{T}}_{\frac{1}{2},xx}] & [\widetilde{\mathbf{T}}_{\frac{1}{2},xy}]\\ [\widetilde{\mathbf{T}}_{\frac{1}{2},yx}] & [\widetilde{\mathbf{T}}_{\frac{1}{2},yy}]\end{bmatrix} \tag{10}$$

which can be linearized when either λ_x or λ_y is constant following [14]. For the "+" branch, we solve

$$\lambda_y \text{ fixed} \Rightarrow \left([\widetilde{\mathbf{T}}_{\frac{1}{2},xx}] + [\widetilde{\mathbf{T}}_{\frac{1}{2},xy}][\mathbf{Q}_y][\widetilde{\mathbf{T}}_{\frac{1}{2},yx}]\right)\mathbf{F}_x = \lambda_x\mathbf{F}_x \tag{11}$$

$$\lambda_x \text{ fixed} \Rightarrow \left([\widetilde{\mathbf{T}}_{\frac{1}{2},yy}] + [\widetilde{\mathbf{T}}_{\frac{1}{2},yx}][\mathbf{Q}_x][\widetilde{\mathbf{T}}_{\frac{1}{2},xy}]\right)\mathbf{F}_y = \lambda_y\mathbf{F}_y . \tag{12}$$

with the matrix $[\mathbf{Q}_\nu]$ defined as

$$[\mathbf{Q}_\nu] = \left(\lambda_\nu[\mathbf{I}] - [\widetilde{\mathbf{T}}_{\frac{1}{2},\nu\nu}]\right)^{-1} . \tag{13}$$

For the "−" branch, we replace λ_x by $-\lambda_x$ in (11)-(13) above. Note that, due to the Euler identity (5), this is equivalent to shifting the scanned path of the "+" mode in x by π.

TABLE II
GEOMETRY PARAMETERS.

Variable	Meaning	Value [mm]
p	periodicity	3.2
$\hat{p}$	glide periodicity	1.6
g	gap	0.05
h	hole depth	1
r	hole radius	1.28

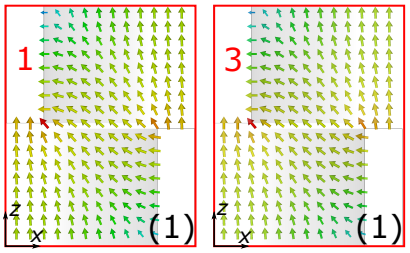

(a)

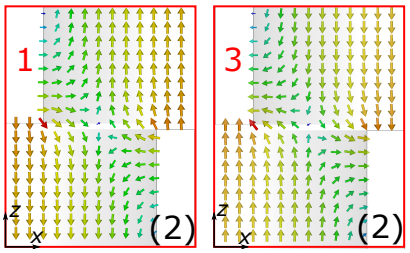

(b)

Fig. 3. Electric field of port modes at y-aligned ports 1 and 3 (in red), with port locations illustrated in Fig. 2, for (a): first and (b): second port modes (port mode numbers in brackets).

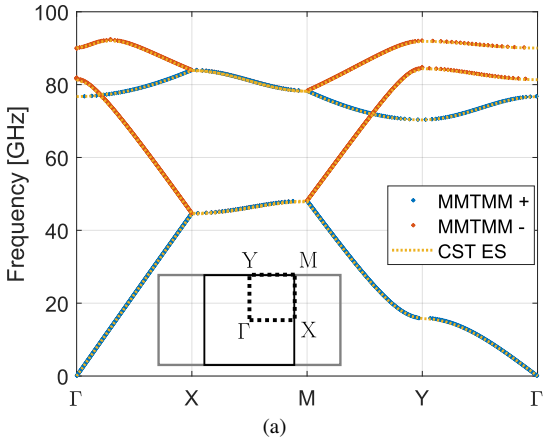

(a)

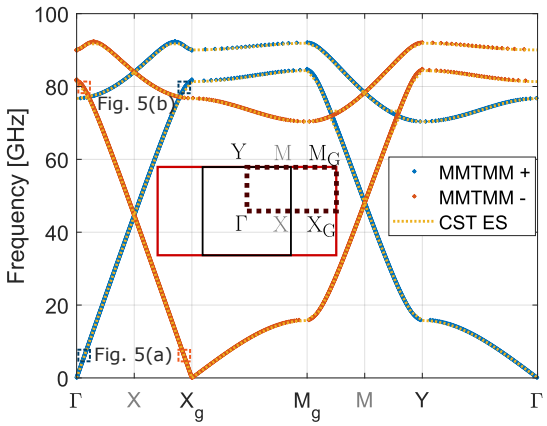

(b)

Fig. 4. Results for the two paths of the glide-symmetric structure: (a) commonly scanned path and (b) proposed path.

IV. RESULTS

Here, we present the results for the example of a 1D glide-symmetric holey structure in Fig. 2. The results are obtained with both CST Eigenvalue Solver (CST ES) for the full cell on the left of Fig. 2, and with MMTMM using 7 modes at each port and the half-cell on the right of Fig. 2. The values and meaning of the variables are given in Table II.

First, the definition of the matrix $[\mathbf{P}]$ is obtained by comparing the z-components of the electric field at two opposite ports. An example of this is shown in Fig. 3. By comparing the left and right sides of Fig. 3(a), we can observe that the two electric fields are in phase, thus making the corresponding entry in $[\mathbf{P}]$ equal to $+1$. In contrast, the fields in Fig. 3(b) are $180°$ out of phase, which makes the entry in $[\mathbf{P}]$ equal to -1. After repeating this process for every port, we obtain

$$[\mathbf{P}] = \mathrm{diag}(\{\mathbf{p}_x, \mathbf{p}_x, \mathbf{p}_y, \mathbf{p}_y\}) \tag{14}$$

with

$$\mathbf{p}_x = \{-1, 1, 1, -1, -1, -1, 1\} \tag{15}$$

$$\mathbf{p}_y = \{1, -1, 1, 1, 1, 1, 1\}\,. \tag{16}$$

Note that these values might change based on the port mode solver type and settings and must always be determined when a new set of coupling matrices is obtained.

The dispersion diagrams of the propagating modes obtained for the commonly scanned path and the proposed path are shown in Fig. 4. The scanned path is depicted in dotted lines in the inset. In Fig. 4(b), we can clearly observe that the "$-$" mode repeats the information in the "$+$" mode in the paths $\overline{\Gamma \mathrm{X_G}}$ and $\overline{\mathrm{M_G Y}}$ when accounting for the shift of π of the scanned path in the Brillouin zone. This is further corroborated by comparison of the surface current in the structure at the same frequency. When we compare the surface current of the "$+$" and "$-$" modes, near Γ, and $\mathrm{X_G}$ (marked in Fig. 4(b) with dashed squares) in Fig. 5, we can observe that they possess the same pattern.

Another aspect of this analysis is an easier comparison of the unit cells to non glide-symmetric ones. In Fig. 6, we compare the "$+$" mode of the glide-symmetric unit cell to the mirror-symmetric unit cell with the same geometrical parameters. The figure illustrates that the glide-symmetric structure lacks a stopband in all directions, yet it exhibits the broadest stopband bandwidth along $\overline{\mathrm{Y\Gamma}}$. Moreover, there is a minor stopband present in the $\overline{\mathrm{X_G M_G}}$ direction. This property may be obscured when observing the results in Fig. 4(a), as the stopband in $\overline{\mathrm{XM}}$ is apparently bigger.

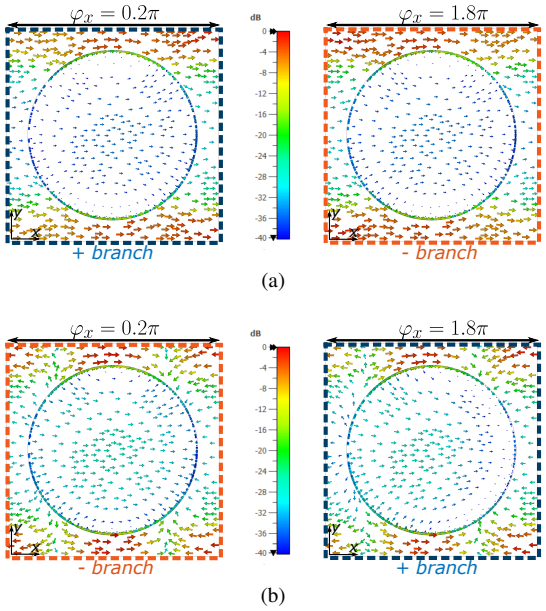

Fig. 5. Surface current on the bottom half of the glide-symmetric unit cell of the: (a): lowest frequency mode, (b): third mode (ordered by frequency).

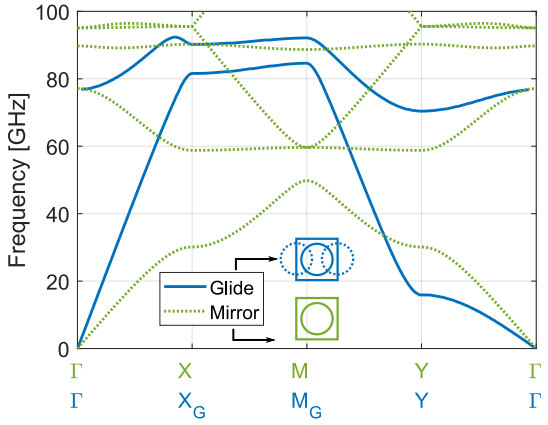

Fig. 6. Comparison of the glide-symmetric unit cell with the mirror-symmetric one with the same geometric parameters.

V. Conclusions

In this study, we introduced an alternative path within the Brillouin zone for one-dimensional glide-symmetric configurations in a two-dimensional square lattice, explicitly taking into account the glide-symmetry periodicity. We demonstrate the concept by implementing a linearized formulation of the MMTMM applied to the half-cell. The proposed path offers several advantages, such as an easier comparison with other geometries, enables better understanding of the anisotropy of the structure, and is computationally more efficient because a reduced unit cell is used.

ACKNOWLEDGEMENT

This publication is in part funded by the Horizon Europe Research and Innovation Program under the GENIUS Project, agreement no. 101072560, and in part by the project PON Research and Innovation "Microwave Imaging and Detection powered by Artificial Intelligence for Medical and Industrial Applications (DM 1062/21)," funded by the MUR, and in part by the project "MedWaveImage - Microwave imaging technology transfer to innovate the medical sector", funded by Interreg Central Europe (CE0200670). It is also supported by Unite! – University Network for Innovation, Technology and Engineering. The work of F. Mesa has been partially supported by the Grant PID2023-148281NB-I00 funded by MICIU/AEI/10.13039/501100011033 and by ERDF/EU.

References

[1] J. D. Joannopoulos, S. G. Johnson, J. N. Winn, and R. D. Meade, *Photonic Crystals*, 2nd ed. New Jersey: Princeton University Press, 2007.

[2] D. M. Pozar, *Microwave Engineering*, 4th ed. New York: John Wiley, 1990.

[3] R. C. Rumpf, "Chapter Three - Engineering the Dispersion and Anisotropy of Periodic Electromagnetic Structures," ser. Solid State Physics, R. E. Camley and R. L. Stamps, Eds. Academic Press, 2015, vol. 66, pp. 213–300.

[4] O. Quevedo-Teruel, Q. Chen, F. Mesa, N. J. Fonseca, and G. Valerio, "On the Benefits of Glide Symmetries for Microwave Devices," *IEEE J. Microw.*, vol. 1, no. 1, pp. 457–469, 2021.

[5] R. Mittra and S. Laxpati, "Propagation in a wave guide with glide reflection symmetry," *Canadian J. Phys.*, vol. 43, no. 2, pp. 353–372, 1965.

[6] S. Amari, R. Vahldieck, and J. Bornemann, "Accurate analysis of periodic structures with an additional symmetry in the unit cell from classical matrix eigenvalues," *IEEE Trans. Microw. Theory Techn.*, vol. 46, no. 10, pp. 1513–1515, 1998.

[7] G. Valerio, F. Ghasemifard, Z. Sipus, and O. Quevedo-Teruel, "Glide-Symmetric All-Metal Holey Metasurfaces for Low-Dispersive Artificial Materials: Modeling and Properties," *IEEE Trans. Microw. Theory Techn.*, vol. 66, no. 7, pp. 3210–3223, 2018.

[8] M. Bagheriasl, O. Quevedo-Teruel, and G. Valerio, "Bloch Analysis of Artificial Lines and Surfaces Exhibiting Glide Symmetry," *IEEE Trans. Microw. Theory Techn.*, vol. 67, no. 7, pp. 2618–2628, 2019.

[9] M. Petek, J. Rivero, J. A. T. Vásquez, G. Valerio, O. Quevedo-Teruel, and F. Vipiana, "Method of Moments for the Dispersion Modeling of Glide-Symmetric Periodic Structures," *IEEE Trans. Antennas Propag.*, vol. 72, no. 1, pp. 756–766, 2024.

[10] A. Hessel, M. H. Chen, R. C. Li, and A. A. Oliner, "Propagation in periodically loaded waveguides with higher symmetries," *Proc. IEEE*, vol. 61, no. 2, pp. 183–195, 1973.

[11] P. Crepeau and P. R. McIsaac, "Consequences of symmetry in periodic structures," *Proc. IEEE*, vol. 52, no. 1, pp. 33–43, 1964.

[12] Z. Sipus, K. Cavar, M. Bosiljevac, and E. Rajo-Iglesias, "Glide-Symmetric Holey Structures Applied to Waveguide Technology: Design Considerations," *Sensors*, vol. 20, no. 23, 2020.

[13] M. Ebrahimpouri, A. Algaba Brazalez, L. Manholm, and O. Quevedo-Teruel, "Using Glide-Symmetric Holes to Reduce Leakage Between Waveguide Flanges," *IEEE Microw. Wireless Compon. Lett.*, vol. 28, no. 6, pp. 473–475, 2018.

[14] F. Giusti, Q. Chen, F. Mesa, M. Albani, and O. Quevedo-Teruel, "Efficient Bloch Analysis of General Periodic Structures With a Linearized Multimodal Transfer-Matrix Approach," *IEEE Trans. Antennas Propag.*, vol. 70, no. 7, pp. 5555–5562, 2022.

[15] J. D. Joannopoulos, S. G. Johnson, J. N. Winn, and R. D. Meade, "Molding the flow of light," *Princet. Univ. Press. Princeton, NJ [ua]*, vol. 12, 2008.

[16] F. Mesa, G. Valerio, R. Rodriguez-Berral, and O. Quevedo-Teruel, "Simulation-Assisted Efficient Computation of the Dispersion Diagram of Periodic Structures: A comprehensive overview with applications to filters, leaky-wave antennas and metasurfaces," *IEEE Antennas Propag. Mag.*, vol. 63, no. 5, pp. 33–45, 2020.

[17] S. Yang, F. Mesa, O. Zetterstrom, S. Clendinning, and O. Quevedo-Teruel, "Understanding the Dispersion Diagrams of Two-Dimensional Supercells," in *2022 Microwave Mediterranean Symposium (MMS)*, 2022, pp. 1–4.